Chemical Engineering Journal 158 (2010) 571–577

Contents lists available at ScienceDirect

Chemical Engineering Journal

journal homepage: www.elsevier.com/locate/cej

Photocatalytic degradation of dyes over combustion-synthesized $Ce_{1-x}Fe_xVO_4$

Parag A. Deshpande, Giridhar Madras*

Department of Chemical Engineering, Indian Institute of Science, Bangalore 560012, India

ARTICLE INFO

Article history:
Received 28 October 2009
Received in revised form 22 January 2010
Accepted 27 January 2010

Keywords:
Orthovanadates
Base-metal substitution
Dye degradation
Combustion synthesis

ABSTRACT

Fe-substituted $CeVO_4$ was synthesized by the solution combustion technique and characterized by X-ray diffraction, X-ray photoelectron spectroscopy, UV–vis spectroscopy, transmission electron microscopy and BET surface area analyzer. These compounds crystallized in tetragonal zircon structure with Fe substituted in ionic state for Ce^{3+} ions. The degradation of anionic and cationic dyes was studied over Fe-substituted $CeVO_4$ compounds. The compounds showed high photocatalytic activity towards dye degradation. The effect of amount of substitution was studied by varying the Fe substitution from 1 to 10%. The rates decreased with increasing substitution of Fe in $CeVO_4$ and 1% Fe substituted $CeVO_4$ showed the highest photocatalytic activity.

1. Introduction

Dyes present in the industrial waste water can pose severe environmental problems and their direct effects on human physiology are well reported [1–9]. The dyes like malachite green have been found to be highly cytotoxic for the mammalian tissues [7–8]. The organic groups present in dyes result in the formation of certain reactive intermediates, which trigger the morphological and genetic alterations, thereby making the dye cytotoxic and carcinogenic. Recently, Inoue et al. [10] showed the carcinogenicity of anthraquinone dyes and the structure of the dye was found to have an influence over the target organs [10–12]. Therefore, the removal of the dyes from industrial waste water becomes important.

Because the traces of the chemicals present in the dye are capable of imparting adverse physiological effects, it becomes necessary to completely remove the toxic materials. Although a number of methods including chemical and wet air oxidation [13–16], catalytic processes [17–18], biochemical processes [19–21] and physical adsorption [22–24] are used for the removal of dyes from the solution, photocatalysis is a promising method to remove the final traces of the hazardous chemicals.

Conventionally, photocatalysis involved the use of semiconductor materials, which mainly included oxides like TiO_2, WO_3, ZnO and certain sulfides like ZnS and CdS [25]. Karunakaran et al. [26–28] have investigated the photocatalytic activity of a range of semiconductor materials for the photocatalytic degradation of various organics. TiO_2 is the most widely used photocatalytic material for the degradation of organics and dyes present in water. Several modifications of TiO_2 have been carried out to observe the changes in the photocatalytic activity. We have previously reported the photocatalytic activity of unsubstituted, impregnated and metal ion substituted TiO_2 for photocatalytic degradation of dyes [29–31]. According to Coleman et al. [32], the generalization of the effect of metals on the photocatalytic activity is not possible and the activity depends upon several factors including the nature of the dye, metal, metal-loading, and the reactant concentration. Therefore, the modification of the parent photocatalytic material by various techniques has been examined. Surface modifications as well as bulk modification, by introducing chemical elements, has been reported to enhance the photocatalytic activity [33–39]. Apart from anatase TiO_2, there have been studies on the photocatalytic activity of perovskites [40–43] and non-stoichiometric perovskites [44].

Orthovanadates have been used as pigments due to the ease of charge transfer [45]. This property also makes them a possible candidate for photocatalytic material and a range of vanadates with different metal ions has been studied for their photocatalytic activity. The degradation of dyes in presence of metal substituted orthovandates has also been investigated [46]. Mahapatra et al. [47] have shown the degradation of dyes and organic compounds over Mo modified Ce, Pr and Nd vanadates. Several other authors have shown the photocatalytic activity of orthovanadates [48–50].

Orthovandates have been synthesized using various techniques including solid-state synthesis [51], microwave synthesis [52], hydrothermal method [53,54] and *chemie douce* [55]. The crystallite size of the catalyst can be controlled to nanometer range using the solution combustion technique. This imparts various important characteristics to the material including high surface area, which are beneficial for catalysis. Bellakki et al. [56] have used the solution combustion technique for the synthesis of $CeVO_4$ and Pd ion substituted $CeVO_4$. They have reported complete substitution of Pd

* Corresponding author. Tel.: +91 80 2293 2321; fax: +91 80 2360 0683.
E-mail address: giridhar@chemeng.iisc.ernet.in (G. Madras).

1385-8947/$ – see front matter © 2010 Elsevier B.V. All rights reserved.
doi:10.1016/j.cej.2010.01.056

ions in Ce^{3+} sites upto 2 at% and the compounds showed high catalytic activity towards the degradation of dyes. The rates achieved over the synthesized catalysts were higher than the rates observed over the commercial TiO_2 catalyst. The substitution of Pd ions was found to enhance the photocatalytic activity. The substitution of a base metal instead of Pd reduces the cost of the catalyst and makes it a possible alternative material for photocatalysis.

In the current study, the photocatalytic degradation of anionic and cationic dyes over combustion-synthesized base metal substituted cerium orthovanadates was investigated. We refer to the term degradation as decolorization/decomposition of the dye in the solution. The basic structure of the dye is broken by the above process. However, the total organic carbon or CO_2 evolution was not measured. Previously [46], it was shown that Fe-substituted $CeVO_4$ synthesized by solid state is capable of degrading dyes. In this study, we show higher photocatalytic activity of Fe-substituted $CeVO_4$ synthesized by solution combustion for the degradation of dyes. The effect of percentage of Fe substitution in $CeVO_4$ on the photocatalytic activity was also studied. The rates were compared with those of commercial Degussa P-25 TiO_2 and substituted $CeVO_4$ synthesized by other methods.

2. Experimental

2.1. Catalyst synthesis and characterization

All the catalysts were synthesized by the solution combustion technique. The precursor solution was made by dissolving ceric ammonium nitrate ($(NH_4)_2Ce(NO_3)_6$, Merck, India), ammonium vanadate (NH_4VO_3, S.D. Fine, India), iron (III) nitrate nonahydrate ($Fe(NO_3)_3{\cdot}9H_2O$, S.D. Fine, India) and oxalyldihidrazide ($C_2H_6N_2O_4$, Alfa Aesar, India) in deionized water. The molar ratio of ceric ammonium nitrate, ammonium vanadate, iron (III) nitrate nonahydrate, and oxalyldihidrazide was $1-x{:}1{:}x{:}2.65$, where x represents the atom% substitution. In the current study, 1%, 2%, 5% and 10% Fe-substituted compounds ($x = 0.01$, 0.02, 0.05 and 0.10, respectively) were synthesized. No iron (III) nitrate nonahydrate was added to the solution for synthesizing (unsubstituted) $CeVO_4$. The solution was heated in a preheated muffle furnace at 350 °C. The catalysts were formed as a result of the spontaneous combustion of the solution. Further details for the synthesis of combustion-synthesized $CeVO_4$ are described elsewhere [56].

The catalysts were characterized by powder X-ray diffraction (XRD), X-ray photoelectron spectroscopy (XPS), UV–vis spectroscopy and BET surface area analyzer. The XRD of the samples were recorded on a Phillips X'pert diffractometer with Cu Kα radiations in a 2θ range of 5–90°. The XPS were recorded on Thermo Fisher Scientific Multilab 2000 (England) instrument with Al Kα radiation (1486.6 eV). C 1s peak at 284.5 eV was used a reference for calibrating the binding energies. The UV–vis spectra were recorded on Lambda 32, PerkinElmer spectrophotometer. The TEM images of the compounds were recorded on JEOL 200CX TEM machine. The surface areas of the compounds were determined using NOVA-1000, Quantachrome apparatus with nitrogen as adsorbent.

2.2. Photoreactor and reactions

The setup for conducting the photocatalytic degradation of dyes consisted of a jacketed flask of capacity 150 ml in which the dye solution along with the catalyst and a magnetic pellet were placed. A high pressure mercury lamp (Philips (125 W), India) placed in a jacketed quartz tube was used as the source of UV radiation. The UV lamp radiated predominantly at 365 nm with a photon flux of 1000 $\mu W\,cm^{-2}$. The dye solution was present in the annulus between the two flasks. Both the flasks were circulated with cold water to remove the heat generated by the lamp. Further details are provided elsewhere [29].

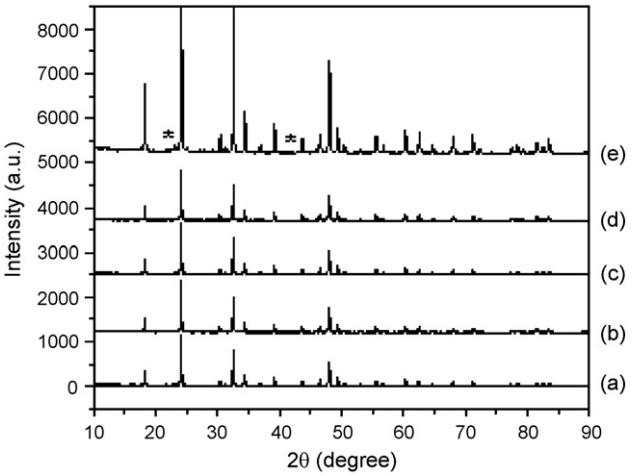

Fig. 1. X-ray diffraction pattern of (a) $CeVO_4$, (b) $Ce_{0.99}Fe_{0.01}VO_4$, (c) $Ce_{0.98}Fe_{0.02}VO_4$, (d) $Ce_{0.95}Fe_{0.05}VO_4$, (e) $Ce_{0.90}Fe_{0.10}VO_4$. The impurity peaks corresponding to α-Fe_2O_3 are marked by asterisks.

Three anionic dyes, Orange G (OG), Remazol Brilliant Blue R (RBBR), Alizarin Cyanine Green (ACG), and three cationic dyes, Methyl Violet (MV), Rhodamine 6G (R6G), and Malachite Green (MG) were chosen for analysis. 100 ml of 50 ppm dye solution was added with 100 mg of the catalyst and stirred using a magnetic stirrer. The solution was stirred in the absence of UV light for 1 h to observe the adsorption of the dye over the catalyst surface. The solution was then irradiated with UV light and the samples were taken for analysis at regular interval of time. The samples were then centrifuged and analyzed using UV–vis spectrophotometer (UV 1700, Shimadzu, Japan). All the reactions were carried out at the natural pH of the dyes. The pH of the solutions was measured before and after adding the catalysts. All the solutions were found to have pH between 6 and 7 and no appreciable change in pH was observed after the addition of the catalysts. Dye samples of known concentrations were prepared and their absorbance was measured. The variation of absorbance with concentration was plotted. The calibration was found to be linear. The variation of the dye concentration with time was determined from the calibration.

3. Result and discussion

3.1. Structural studies

The unsubstituted and Fe-substituted $CeVO_4$ compounds crystallized as single phase solid solutions with tetragonal zircon structure. Fig. 1(a) shows the XRD of $CeVO_4$. All the diffraction lines in the XRD of $CeVO_4$ could be indexed to the zircon structure with space group $I4_1/amd$. The XRD of the Fe substituted $CeVO_4$ gave no additional peak up to 5 at% substitution (Fig. 1(b–d)). Additional peaks can be seen in the XRD on 10 at% substitution (Fig. 1(e)). Therefore, at lower substitutions, Fe ions were substituted in Ce^{3+} sites and the zircon structure of $CeVO_4$ was retained. In a previous study, we have found the upper limit of substitution of Fe ions in $CeVO_4$ to be 5% owing to high lattice distortion on higher substitution [46].

The XPS of the elements were recorded to obtain the information about the oxidation state of the compounds. XPS of Ce 3d showed the presence of Ce^{3+} ions (see Supplementary information, Fig. S1) and the presence of V in +5 state (see Supplementary information, Fig. S2) in all the compounds. The XPS of Fe 3d is shown in Fig. 2(a). Fe in $Ce_{0.99}Fe_{0.01}VO_4$ was present in +2 state. At higher substitu-

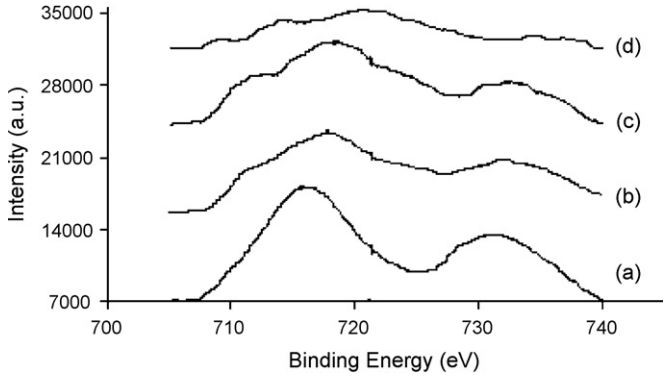

Fig. 2. X-ray photoelectron spectra of Fe in (a) $Ce_{0.99}Fe_{0.01}VO_4$, (b) $Ce_{0.98}Fe_{0.02}VO_4$, (c) $Ce_{0.95}Fe_{0.05}VO_4$, (d) $Ce_{0.90}Fe_{0.10}VO_4$.

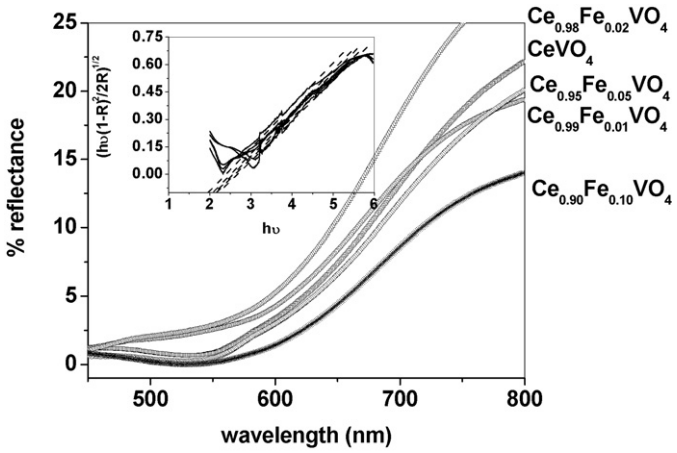

Fig. 3. Diffuse reflectance spectra of the various synthesized compounds. The inset in the figure shows the Kubelka–Munk plot.

tions, Fe in +3 state was also observed. Distinct peaks at 720 eV can be observed in the spectra of $Ce_{0.95}Fe_{0.05}VO_4$ and $Ce_{0.90}Fe_{0.10}VO_4$ (Fig. 2(b–d)) corresponding to Fe in +3 state. The relative composition of Fe^{2+}:Fe^{3+} was found by decomposing the XPS into the various states of Fe. The areas of the peaks corresponding to +2 and +3 states signified the amount of Fe present in that state. Fe^{3+} was present in maximum amount in $Ce_{0.90}Fe_{0.10}VO_4$. Nearly 30% of Fe was in +3 state (Table 1). In the XPS of $Ce_{0.90}Fe_{0.10}VO_4$, peaks are wide showing the presence of multiple oxidation state. Fig. 2 shows the shift in the peaks that can be observed in the spectra with the increase in percentage of Fe substitution and peaks at 720 eV (corresponding to Fe in +3 state) emerge very clearly in the spectra of $Ce_{0.90}Fe_{0.10}VO_4$. Clearly, with an increase in the substitution, the amount of Fe^{3+} in the compounds increased. As mentioned earlier, impurity peaks corresponding to Fe_2O_3 (where Fe is in +3) was observed for the case of $Ce_{0.90}Fe_{0.10}VO_4$.

The ionic radii of Fe and Ce ions follow the order $Ce^{3+} > Fe^{2+} > Fe^{3+}$. Therefore, for lattice matching, Fe remains in +2 state. However, in the precursor, the oxidation state of Fe is +3. As a result, the amount of Fe in +3 state in the compound increases with increase in percentage of substitution.

The diffuse reflectance spectra of all the compounds were recorded to determine the band gap. Fig. 3 shows the spectra for $CeVO_4$ and Fe substituted $CeVO_4$. The band gap of the compound was determined from the absorption edge. The relation between the absorption edge and the band gap of the material is given as $E_g = 1240/\lambda$, where λ corresponds to the wavelength (in nm) of the absorption edge [57]. The inset in Fig. 3 shows the Kubelka–Munk plot [58]. The dotted line in the figure shows the extrapolation used for determining the band gap. The band gaps of all the compounds are given in Table 1. The band gap of $CeVO_4$ was found to be 2.11 eV. The band gap remained unchanged at lower substitutions with a value of 2.12 eV and 2.11 eV for $Ce_{0.99}Fe_{0.01}VO_4$ and $Ce_{0.98}Fe_{0.02}VO_4$, respectively. However, the band gap decreased with increase in substitution and decreased to a value of 2.02 eV on 10% Fe substitution. The underlying principle for change of the band gap of the solids is the same as that used for enhancing the conductivity of the semiconductor by doping an aliovalent atom. The introduction of an impurity results in creation of defects in the solids. Due to this, the defect band appears and the band gap reduces. Zhang et al. have observed a reduction of the band gap in perovskites on introduction of Fe impurities [59]. Similarly, Liu et al. [60] have observed a reduction in the band gap of ZnS and CdS semiconductors by formation of solid solutions of the type $Cd_{1-x-y}Fe_xZn_yS$. The band gap decreased with increase in Fe content. This has been to attributed to the decrease in the band gap to the Fe^{2+}/Fe^{3+} transitions [61]. Solid state synthesized $Ce_{0.95}Fe_{0.05}VO_4$ showed a band gap of 2.9 eV [46]. The band gap for tetragonal structured lanthanum orthovanadates synthesized by solution-based method showed a band gap of 2.74 eV, 2.86 eV, and 2.99 eV for $CeVO_4$, $PrVO_4$ and $NdVO_4$, respectively [51]. Bi based tetragonal orthovanadates have been reported to have a band gap of 2.9 eV [48]. Therefore, the band gap for the combustion-synthesized compounds is lesser as compared to the other similar compounds synthesized by other methods. The use of combustion synthesis results in the introduction of carbon in the structure of the compound and a solid solution of the synthesized compound with carbon is formed. This results in the lowering of the band gap. This phenomenon has been illustrated by Khan et al. [62] for modified TiO_2 compounds synthesized by combustion of Ti metal in a natural gas flame. We have previously reported similar findings on combustion-synthesized TiO_2 where the band gap was found to be lower as compared to those synthesized with other methods [63].

The TEM image and the electron diffraction pattern of $Ce_{0.99}Fe_{0.01}VO_4$ are shown in Fig. 4. The particle size of 10–20 nm can be observed from the TEM image. No bulk aggregation was observed and the TEM images also confirm that Fe was substituted in the lattice.

The BET surface areas of all the compounds were determined. Table 1 gives the surface areas of all the synthesized compounds. The surface area of $CeVO_4$ was 22 m^2/g. The surface area remained unchanged on small amount of Fe substitution and the surface areas of $Ce_{0.99}Fe_{0.01}VO_4$ and $Ce_{0.98}Fe_{0.02}VO_4$ were nearly the same as that of $CeVO_4$. However, the areas decreased with increase in substitution and $Ce_{0.90}Fe_{0.10}VO_4$ had a surface area of 10 m^2/g.

Table 1
Various combustion-synthesized compounds with crystal structure, Fe ionic state, band gap and surface area.

Compound	Crystal structure	Fe ionic state (Fe^{2+}:Fe^{3+})	Band gap (eV)	Surface area (m^2/g)
$CeVO_4$	Zircon ($I4_1/amd$)	–	2.11	22
$Ce_{0.99}Fe_{0.01}VO_4$	Zircon ($I4_1/amd$)	Ionic (Fe^{2+} > 97%)	2.12	22
$Ce_{0.98}Fe_{0.02}VO_4$	Zircon ($I4_1/amd$)	Ionic (80:20)	2.11	22
$Ce_{0.95}Fe_{0.05}VO_4$	Zircon ($I4_1/amd$)	Ionic (64:36)	2.08	14
$Ce_{0.90}Fe_{0.10}VO_4$	Zircon ($I4_1/amd$)	Ionic (31:69)	2.02	10

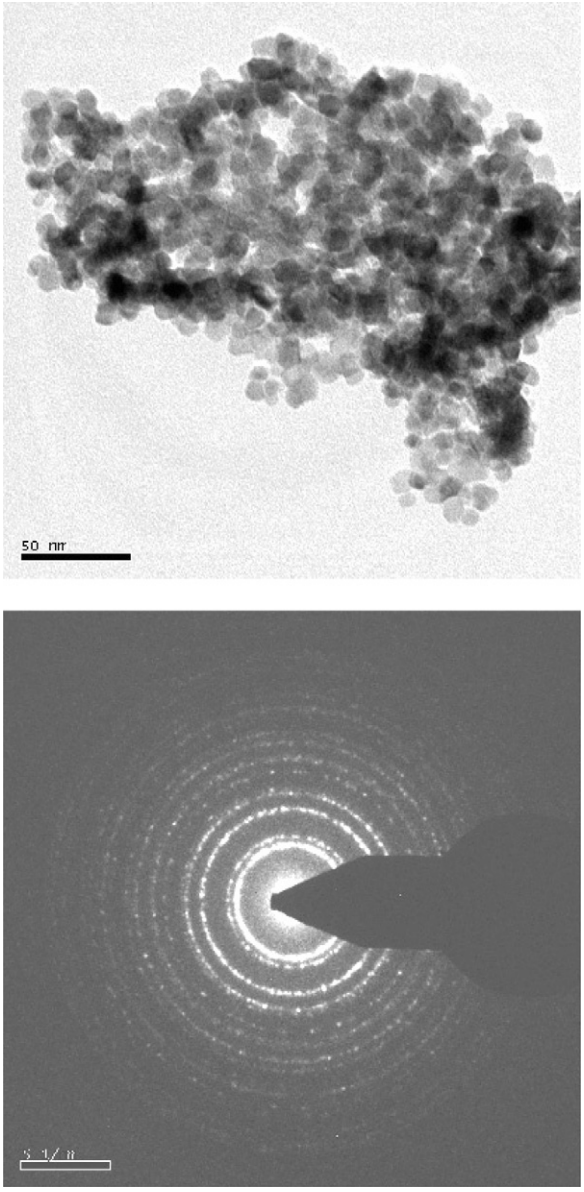

Fig. 4. TEM images of $Ce_{0.99}Fe_{0.01}VO_4$ with the electron diffraction pattern.

3.2. Photocatalytic degradation studies

Photocatalytic degradation of dyes was carried over the commercial Degussa P-25 catalyst, $CeVO_4$ and Fe-substituted $CeVO_4$. The combustion-synthesized compounds showed high activity towards photocatalytic degradation. The degradation experiments were first carried out with commercial Degussa P-25 catalyst. Fig. 5 shows the degradation profile of the different dyes over the various catalysts tested. The variation of the normalized dye concentration time is plotted against time. The initial concentration for normalization was the concentration of the dye obtained after stirring the dye solution for 1 h. During this period, the adsorption of the dye was less than 5% of the initial concentration. It can be seen from Fig. 5 that Fe-substituted compounds showed higher activity for dye degradation as compared to the commercial Degussa P-25 TiO_2 and $CeVO_4$. The activity of the catalysts decreased with increasing %Fe substitution. $Ce_{0.99}Fe_{0.01}VO_4$ was the best catalyst. More than 95% conversion of all the dyes was achieved over $Ce_{0.99}Fe_{0.01}VO_4$ within 30 min.

The Langmuir–Hinshelwood (LH) kinetic model is the conventionally used model to describe the kinetics of photocatalytic degradation of dyes. The expression describing the rate of reaction as a function of dye concentration can be written as $r = k_r K_a C/(1 + K_a C)$, where r is the rate of reaction, k_r is the reaction rate constant, K_a is the equilibrium constant, and C is the concentration of the dye. The intermediate processes involved in the reaction include the electron–hole pair generation, adsorption of the dye over the catalyst surface, hydroxyl and superoxide radical generation and the attack of dyes by these radicals [25]. When the initial concentration of the dye is small (millimolar) (i.e. when $K_a C \ll 1$), this equation can be approximated as a first order process whose rate is given as $r = k_{app} C$, where k_{app} is the pseudo-first order reaction rate constant describing the rate of the reaction. In our previous studies also, we have found the LH parameter to be significantly lesser than the kinetic parameter and the degradation could be described as a first order process [64,65]. Using the above rate expression, the variation of the dye concentration with time is given as $C = C_0 \exp(-k_{app} t)$, where C_o is the initial dye concentration. The lines in Fig. 5 correspond to the first order degradation model given by the above equation.

The variation of the natural log of the normalized concentration C/C_o with time followed a linear trend (see Supplementary information, Fig. S3). The lines in the figure show the least square linear fit of the data. The reaction rate constant was obtained by the slope of the line. The values of the rate constants for the various catalysts are given in Table 2. It can be seen from Table 2 that the rate constants were the highest for $Ce_{0.99}Fe_{0.01}VO_4$. For all the dyes, the rate constants decreased with increase in Fe substitution but were always higher than that of the $CeVO_4$. For the degradation of cationic dyes, the activity of $Ce_{0.99}Fe_{0.01}VO_4$.was higher than that observed with Degussa P-25.The anionic dyes were found to degrade faster as compared to the cationic dyes. The degradation of anionic dyes over $Ce_{0.99}Fe_{0.01}VO_4$ was 10–20 times higher than that over the commercial Degussa P-25 catalyst. All the combustion-synthesized compounds showed higher activity for the degradation of anionic dyes than Degussa P-25. $CeVO_4$ also showed photocatalytic activity that was 2–3 times higher than that of Degussa P-25.

Having established the high activity of the combustion-synthesized compounds, the reactions were carried out for a longer period by irradiating the solution for 2 h. Fig. S4 (see Supplementary information) shows the variation of the dye concentration for different initial concentration with time over $Ce_{0.95}Fe_{0.05}VO_4$. More than 95% degradation of the dyes was possible for all the initial concentration of dyes. It was found that most of the degradation occurred in first 60 min for all the dyes. At higher concentrations, the time requirement for degradation to the same percentage of conversion increased. Whereas more than 90% degradation was observed within 20 min for most of the dyes with an initial concentration of 25 ppm, the time requirement for the same conversion was more than 1 h for reactions with an initial concentration of 100 ppm. Fig. S5 (see Supplementary information) shows the variation of the normalized dye concentration over unsubstituted and Fe-substituted compounds irradiated for 2 h. It can be seen that the $CeVO_4$ showed much lesser activity than Fe-substituted compounds. Complete degradation of all the anionic dyes took place within 2 h.

The activity of Fe-substituted compounds was higher than that of the Pd-substituted compound synthesized by the same solution combustion method. Bellakki et al. [56] reported the degradation of OG and RBBR over Pd-substituted compound. By comparison of the first order reaction rate constants for the degradation of OG and RBBR in presence of Pd-substituted and Fe-substituted compounds, it can be seen that the degradation was 3–4 times faster over Fe-substituted compounds (Table 3). Similarly, the rates of degradation for OG and RBBR were higher over combustion-

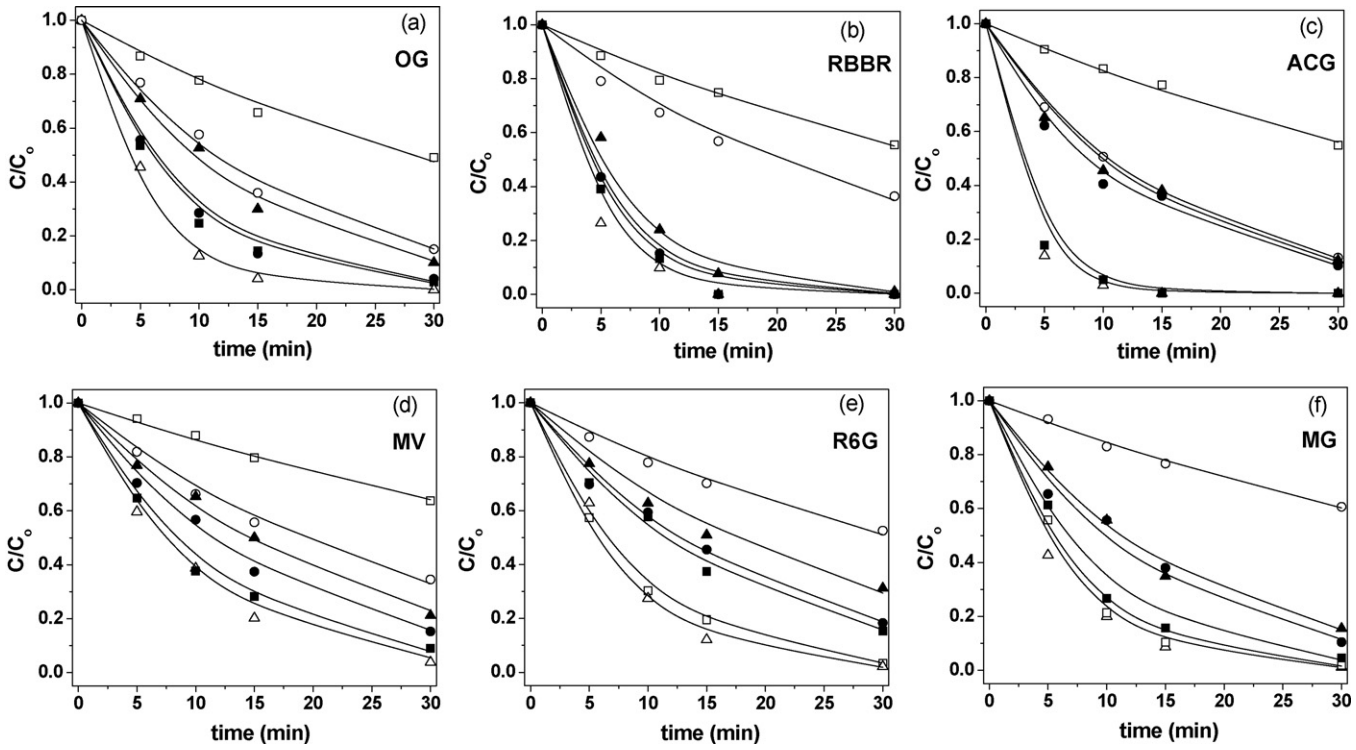

Fig. 5. Variation of the normalized dye concentration with time for the degradation of various dyes over the different catalysts. (a) OG, (b) RBBR, (c) ACG, (d) MV, (e) R6G, (f) MG. (□) Degussa P-25 TiO_2, (○) $CeVO_4$, (△) $Ce_{0.99}Fe_{0.01}VO_4$, (■) $Ce_{0.98}Fe_{0.02}VO_4$, (●) $Ce_{0.95}Fe_{0.05}VO_4$, (▲) $Ce_{0.90}Fe_{0.10}VO_4$.

Table 2
Pseudo-first order rate constants k ($min^{-1} \times 10^3$) for the degradation of the various dyes over the different catalysts.

	Degussa P-25	$CeVO_4$	$Ce_{0.99}Fe_{0.01}VO_4$	$Ce_{0.98}Fe_{0.02}VO_4$	$Ce_{0.95}Fe_{0.05}VO_4$	$Ce_{0.90}Fe_{0.10}VO_4$
OG	25	63	207	124	116	75
RBBR	20	35	239	200	184	155
ACG	19	68	362	308	76	72
MV	15	37	97	85	62	49
R6G	112	22	133	62	56	41
MG	139	17	154	110	72	63

synthesized Fe-substituted $CeVO_4$ as compared to the degradation over Fe-substituted $CeVO_4$ synthesized by solid state method [46]. Combustion-synthesized $CeVO_4$ showed an activity that was six times higher than that of solid state synthesized $CeVO_4$. Similarly, for the same percentage of substitution, combustion-synthesized Fe-substituted compounds showed activity that was 2–4 times higher than that of Li substituted compounds synthesized by solid state method [46].

The combustion-synthesized compounds show high crystallinity with crystallites in nanometer range [66]. Owing to this, the compounds show high surface area. The surface area of $CeVO_4$ synthesized by solution combustion technique was found to be 15–20 times higher than that synthesized by solid state methods. The increase in surface area of the compound had a direct effect over the photocatalytic activity of the compound. The surface area of the compounds decreased with an increase in percentage of Fe substitution. The effect of this was reflected in the photocatalytic activity of the compounds and the activity of the compounds followed the order, $Ce_{0.99}Fe_{0.01}VO_4 > Ce_{0.98}Fe_{0.02}VO_4 > Ce_{0.95}Fe_{0.05}VO_4 > Ce_{0.90}Fe_{0.10}VO_4$. However, the surface areas of unsubstituted, 1% and 2% Fe-substituted compounds were similar. The difference in activity of these compounds can be explained in the basis of the various redox processes that occur during the reaction.

In the reducible oxides, various redox couples are observed. In $CeVO_4$, oxidation and reduction of Ce and V occur in the reducing and oxidizing environment and $Ce^{3+} \leftrightarrow Ce^{4+}$ and $V^{5+} \leftrightarrow V^{4+}$ are observed. XPS showed the initial oxidation state of Ce and V to be +3 and +5, respectively (see Supplementary information, Figs. S1 and S2). Therefore, oxidation of Ce to +4 and reduction of V to +4 can

Table 3
First order rate constants for the degradation of dyes over different orthovanadates synthesized by various techniques.

Compound	Method of synthesis	Dye	k ($min^{-1} \times 10^3$)
$Ce_{0.98}Pd_{0.02}VO_4$	Combustion synthesis	OG	39
		RBBR	48
$CeVO_4$	Solid state synthesis	OG	10
		RBBR	5
$Ce_{0.90}Li_{0.10}VO_4$	Solid state synthesis	OG	32
		RBBR	40

take place. However, introduction of Fe in the compound induces additional redox couples and $Fe^{3+} \leftrightarrow Fe^{2+}$ can be expected. In the compounds in which Fe is substituted in fully oxidized +3 state, Ce is in reduced +3 state and V is in oxidized +5 state. Thus, the same redox couples are formed as in case of $CeVO_4$. Therefore, the introduction of Fe does not have any effect and the accessibility of the redox couples is the same as the accessibility in $CeVO_4$. However, when Fe is substituted in +2 state, the redox processes are enhanced. Oxidation of Fe^{2+} to Fe^{3+} takes place reducing V^{5+} to V^{4+}. During the reduction of Fe^{3+}, oxidation of Ce^{3+} to Ce^{4+} can take place. Therefore, introduction of Fe in +2 state enhanced the redox couples in the compound.

The interaction of Fe ions with the hydroxyl group takes place as $Fe^{3+} + OH^- \rightarrow Fe^{2+} + OH^{\bullet}$ [67]. The above equation shows the formation of reactive hydroxyl radical from the hydroxyl ion by corresponding reduction of Fe^{3+} to Fe^{2+}. Further, a small amount of Fe^{3+} enhances the electron capture and reduces electron–hole recombination [68]. Therefore, the introduction of Fe ions results in an increase in the activity of the compound. The interaction of Fe ions with the support Ce ions is possible due to the reducible nature of the support. High activity of $Ce_{0.99}Fe_{0.01}VO_4$ is possibly due to the formation of redox couples. With increase in substitution, the amount of Fe^{3+} increased and following the arguments given above, the redox processes reduce and the activity decreases. Further, the mechanism of degradation of an organic compound over a photocatalyst involves the generation of electron–hole pairs. This process is fast and reversible. Therefore, the recombination of holes and electrons also takes place releasing heat. At very high Fe-substitution, the metallic character of the compound increases and the conduction band gets populated by electrons covering the band gap. The reduction of band gap and high density of electrons in the conduction band results in lowering of the electron–hole generation and increase the electron–hole recombination. Fe becomes the center for electron–hole recombination and, therefore, a decrease in activity of the catalyst was observed with an increase in Fe substitution. Further, the surface areas decreased as percentage of Fe substitution increased from 2% to 10%. This decrease in surface area also resulted in the reduction of photocatalytic activity.

4. Conclusions

Photocatalytic degradation of anionic and cationic dyes was carried out in presence of unsubstituted and Fe-substituted $CeVO_4$ synthesized by solution combustion technique. The compounds showed high photocatalytic activity and the degradation rates were first order in dye concentration. The rates of degradation were compared with the rates of degradation in presence of commercial Degussa P-25 TiO_2 catalyst. The photocatalytic activity of the compounds was enhanced by substitution of Fe ions. However, the rates of dye degradation decreased with an increase in Fe-substitution and $Ce_{0.99}Fe_{0.01}VO_4$ was found to be the best catalyst. The activity of $Ce_{0.99}Fe_{0.01}VO_4$ was the highest and the degradation over $Ce_{0.99}Fe_{0.01}VO_4$ was faster than the degradation over the commercial TiO_2 catalyst for any of the dyes.

Acknowledgements

The authors acknowledge the Department of Science and Technology, India, for financial support. GM gratefully acknowledges Department of Science and Technology for the Swarnajayanti fellowship. The authors are thankful to Paromita Kundu and Dr. N. Ravishankar of Materials Research Center, IISc, for TEM analysis, Dr. Suresh of CGPL, IISc, for surface area measurements and M. Surekha of NIT Surat for assistance in degradation experiments.

Appendix A. Supplementary data

Supplementary data associated with this article can be found, in the online version, at doi:10.1016/j.cej.2010.01.056.

References

[1] M. Giger, H.R. Baumgartner, G. Zbinden, Toxicological effects of evince blue and congo red on blood platelets, Agents Action 4 (1974) 173–180.
[2] K. Tsuchiya, T. Okubu, S. Ishizu, An epidemiological study of occupational bladder tumours in the dye industry in Japan, Br. J. Ind. Med. 32 (1975) 203–209.
[3] C.R. Nony, M.C. Bowman, T. Cairns, Metabolism studies of an azo dye and pigment in the hamster based in analysis of the urine for potentially carcinogenic aromatic amine metabolites, J. Anal. Toxicol. 4 (1980) 132–140.
[4] R.B. Haveland-Smith, R.D. Combes, B.A. Briges, Studies on the genotoxicity of some fluorescein dyes, Mutat. Res. 88 (1981) 1–15.
[5] R.D. Combes, R.B. Haveland-Smith, A review of the genotoxicity of food, drug and cosmetic colours and other azo, triphenylmethane and xanthane dyes, Mutat. Res. 98 (1982) 101–248.
[6] H. Kosaka, S.I. Nakamura, Genotoxicity of synthetic dyes in umu test using salmonella typhimurium ta1535/pSK1002 (1): results of examination for acid dyes, disperse dyes and reactive dyes, Jpn. J. Ind. Health 32 (1990) 89–104.
[7] A. Panandikar, C. Fernandes, V.K.V. Rao, The cytotoxic properties malachite green are associated with increased demethylase, aryl hydrocarbon hydrolase and lipid peroxidation in primary cultures of syrian hamster embryo cells, Cancer Lett. 67 (1992) 93–101.
[8] A. Panandikar, G.B. Maru, V.K.V. Rao, Dose-response effects of malachite green in free radical formation, lipid peroxidation and DNA damage in syrian hamster embryo cells and their modulation by antioxidants, Carcinogenesis 15 (1994) 2445–2448.
[9] C. Helmes, C.I. Tucker, Disperse Blue 79. Environmental safety and human health effects of this commercially significant dye, Text. Chem. Colorist. 25 (1993) 15–17.
[10] K. Inoue, M. Yoshida, M. Takahashi, H. Fujimoto, K. Ohnishi, K. Nakashima, M. Shibutani, M. Hirise, A. Nishikawa, A possible contribution of rubadin, a metabolite of madder color, to renal carcinogenesis in rats, Food Chem. Toxicol. 47 (2009) 752–759.
[11] A.M. Doi, R.D. Irwin, J.R. Bucher, Influence of functional group substitutions on the carcinogenicity of anthraquinone in rats and mice: analysis of long-term bioassays by the National Cancer Institute and the National Toxicology Program, J. Toxicol. Environ. Health, Part B 8 (2005) 109–126.
[12] Y. Kawasaki, Y. Goda, K. Yoshihira, The mutagenic constituents of *Rubia tinctorum*, Chem. Pharm. Bull. 40 (1992) 1504–1509.
[13] B. Gozman, B. Kalyan, A.M. Gizir, A. Hesenov, Oxidative degradations of reactive blue 4 dye by different advance oxidation methods, J. Hazard. Mater. 168 (2009) 129–136.
[14] B.H. Hameed, T.W. Lee, Degradation of malachite green in aqueous solution by Fenton process, J. Hazard. Mater. 164 (2009) 468–472.
[15] L. Lei, Q. Dai, M. Zhou, X. Zhang, Decolorization of cationic red X-GRL by wet-air oxidation: performance optimization and degradation mechanism, Chemosphere 68 (2007) 1135–1142.
[16] Y. Liu, D. Sun, Development of Fe_2O_3-CeO_2-TiO_2/γ-Al_2O_3 as a catalyst for catalytic wet air oxidation of methyl orange azo dye under room conditions, Appl. Catal. B: Environ. 72 (2007) 205–211.
[17] L. Gao, Y. Zhai, H. Ma, B. Wang, Degradation of cationic dye methylene blue by ozonation assisted with kaolin, Appl. Clay Sci. 46 (2009) 226–229.
[18] X. Zhao, B. Zhang, K. Ai, G. Zhang, L. Cao, X. Liu, H. Sun, H. Wang, L. Lu, Monitoring catalytic degradation of dye molecules on silver-coated ZnO nanowire arrays by surface-enhanced Raman spectroscopy, Mater. Chem. 19 (2009) 5547–5553.
[19] H. Wang, J.Q. Su, X.W. Zheng, Y. Tian, X.J. Xiong, T.L. Zheng, Bacterial decolorization and degradation of the reactive dye Reactive Red 180 by *Citrobacter* sp. CK3, Int. Biodeterioration Biodegradation 63 (2009) 395–399.
[20] K.P. Gopinath, H.A.M. Sahib, K. Muthukumar, M. Velan, Improved biodegradation of Congored by using *Bacillus* sp., Bioresour. Technol. 100 (2009) 670–675.
[21] Y.M. Kolekar, S.P. Pawar, K.R. Gawai, P.D. Lokhande, Y.S. Shouche, K.M. Kodam, Decolorization and degradation of Disperse Blue 79 and Acid Orange 10, by *Bacillus fusiformis* KMK5 isolated from the textile dye contaminated soil, Bioresour. Technol. 99 (2007) 8999–9003.
[22] J. Yu, B. Li, X. Sun, Y. Jun, R. Chi, Adsorption of methylene blue and rhodamine B on baker's yeast and photocatalytic regeneration of the biosorbent, Biochem. Eng. J. 45 (2009) 145–151.
[23] D. Mahanta, G. Madras, S. Radhakrishnan, S. Patil, Adsorption and desorption kinetics of anionic dyes on doped polyaniline, J. Phys. Chem. B 113 (2009) 2293–2299.
[24] D. Mahanta, G. Madras, S. Radhakrishnan, S. Patil, Adsorption of sulfonated dyes by polyaniline emeraldine salt and its kinetics, J. Phys. Chem. B 112 (2008) 10153–10157.
[25] M.R. Hoffmann, S.T. Martin, W. Choi, Environmental applications of semiconductor photocatalysis, Chem. Rev. 95 (1995) 69–96.
[26] C. Karunakaran, R. Dhanalakshmi, S. Karuthapandian, Inhibition of photooxidation of iron (II) by some semiconductors, J. Photochem. Photobiol. A 170 (2005) 233–238.
[27] C. Karunakaran, R. Dhanalakshmi, Semiconductor-catalyzed degradation of phenols with sunlight, Sol. Energy Mater Sol. Cells 92 (2008) 1315–1321.

[28] C. Karunakaran, R. Dhanalakshmi, Substituent effects on nano TiO_2- and ZnO-catalyzed phenol photodegradation rates, Int. J. Chem. Kinet. 41 (2009) 275–283.
[29] R. Vinu, G. Madras, Photocatalytic activity of Ag-substituted and impregnated nano-TiO_2, Appl. Catal. A: Gen. 366 (2009) 130–140.
[30] R. Vinu, G. Madras, Synthesis and photoactivity of Pd substituted nano-TiO_2, J. Mol. Catal. A: Chem. 291 (2008) 5–11.
[31] K. Nagaveni, M.S. Hegde, G. Madras, Structure and photocatalytic activity of $Ti_{1-x}M_xO_2 \pm \delta$ (M = W, V, Ce, Zr, Fe and Cu) synthesized by solution combustion method, J. Phys. Chem. B 108 (2004) 20204–20212.
[32] H.M. Coleman, K. Chiang, R. Amal, Effects of Ag and Pt on photocatalytic degradation of endocrine disrupting chemicals in water, Chem. Eng. J. 113 (2005) 65–72.
[33] R. Hong, T. Pan, J. Qian, H. Li, Synthesis and surface modification of ZnO nanoparticles, Chem. Eng. J. 119 (2006) 71–81.
[34] C. Shifu, Z. Wei, Z. Sujuan, L. Wei, Preparation, characterization and photocatalytic activity of N-containing ZnO powder, Chem. Eng. J. 148 (2009) 263–269.
[35] H. Wang, S. Baek, J. Lee, S. Lim, High photocatalytic activity of silver-loaded ZnO-SnO_2 coupled catalysts, Chem. Eng. J. 146 (2009) 355–361.
[36] S. Sakthivel, M.V. Shankar, M. Palanichamy, B. Arabondoo, D.W. Bahnemann, V. Murugesan, Enhancement in photocatalytic activity by metal deposition: characterisation and photonic efficiency of Pt, Au and Pd deposited on TiO_2 catalyst, Water Res. 38 (2004) 3001–3008.
[37] F. Wei, L. Ni, P. Cui, Preparation and characterization of N-S-codoped TiO_2 photocatalyst and its photocatalytic activity, J. Hazard. Mater. 156 (2008) 135–140.
[38] J. Sun, L. Qiao, S. Sun, G. Wang, Photocatalytic degradation of Orange G on nitrogen-doped TiO_2 catalysts under visible light and sunlight irradiation, J. Hazard. Mater. 155 (2008) 312–319.
[39] X. Li, R. Xiong, G. Wei, Preparation and photocatalytic activity of nanoglued Sn-doped TiO_2, J. Hazard. Mater. 164 (2009) 587–591.
[40] J. Kong, A. Li, H. Zhai, H. Li, Q. Yan, J. Ma, D. Wu, Preparation, characterization and photocatalytic properties of $ZnTiO_3$ powders, J. Hazard. Mater. 171 (2009) 918–923.
[41] J. Yin, Z. Zou, J. Ye, A novel series of the new visible-light-driven photocatalyst $MCo_{1/3}Nb_{2/3}O_3$ (M = Ca, Sr, and Ba) with special electronic structures, J. Phys. Chem. B 107 (2003) 4936–4941.
[42] S. Song, L. Xu, Z. He, H. Ying, J. Chen, X. Xiao, B. Yan, Photocatalytic degradation of C.I. Direct Red 23 in aqueous solutions under UV irradiation using $SrTiO_3/CeO_2$ composite as catalyst, J. Hazard. Mater. 152 (2008) 1301–1308.
[43] P. Mahata, T. Aarthi, G. Madras, S. Natarajan, Photocatalytic degradation of dyes and organics with nanosized $GdCoO_3$, J. Phys. Chem. C 111 (2007) 1665– 1674.
[44] G. Zhang, J. Zhau, X. Ding, Y. Hu, J. Xie, Characterization and photocatalytic properties of Ni-doped $Sr_{10}Bi_6O_{24-y}$, J. Hazard. Mater. 158 (2008) 287–292.
[45] M.R. Dolgos, A.M. Paraskos, M.W. Stolzfus, S.C. Yarnell, P.M. Woodward, The electronic structure of vanadate salts: cation substitution as a tool for bandgap manipulation, J. Solid State Chem. 182 (2009) 1964–1971.
[46] S. Mahapatra, R. Vinu, D. Saha, T.N. Guru Row, G. Madras, Synthesis, characterization and photocatalytic activity of $M_xC_{1-x}VO_4$ (M = Li, Ca and Fe), Appl. Catal. A: Gen. 361 (2009) 32–41.
[47] S. Mahapatra, R. Vinu, T.N. Guru Row, G. Madras, Kinetics of photoconversion of cyclohexane and benzene by $LnMo_{0.15}V_{0.85}O_4$ (Ln = Ce, Pr, Nd), Appl. Catal. A: Gen. 351 (2008) 45–53.
[48] S. Tokunaga, H. Kato, A. Kudo, Selective preparation of monoclinic and tetragonal $BiVO_4$ with scheelite and their photocatalytic properties, Chem. Mater. 13 (2001) 4624–4628.
[49] S. Kohtani, J. Hiro, N. Yamamoto, A. Kudo, K. Tokumura, R. Nakagaki, Adsorptive and photocatalytic properties of Ag-loaded $BiVO_4$ on the degradation of 4-n-alkylphenols under visible light irradiation, Catal. Commun. 6 (2005) 185–189.
[50] M. Shang, W. Wang, L. Zhau, S. Sun, W. Yin, Nanosized $BiVO_4$ with high visible-light-indiced photocatalytic activity, ultrasonic assisted synthesis and protective effect of surfactant, J. Hazard. Mater. 172 (2009) 338–344.
[51] S. Mahapatra, G. Madras, T.N. Guru Row, Synthesis, characterization and photocatalytic activity of lanthanide (Ce, Pr, Nd) orthovanadates, Ind. Eng. Chem. Res. 46 (2007) 1013–1017.
[52] S. Mahapatra, S.K. Nayak, G. Madras, T.N. Guru Row, Microwave synthesis and photocatalytic activity of nano lanthalides (Ce, Pr, Nd) orthovanadates, Ind. Eng. Chem. Res. 17 (2008) 6509–6516.
[53] S. Mahapatra, A. Ramanan, Hydrothermal synthesis and structural study of lanthanide orthovanadates, $LnVO_4$ (Ln = Sm, Gd, Dy, Ho), J. Alloys Compd. 395 (2005) 149–153.
[54] X. Wu, Y. Tao, C. Mao, D. Liu, Y. Mao, In situ hydrothermal synthesis of YVO_4 nanorods and microtubes using $(NH_4)_{0.5}V_2O_5$ nanowires templates, J. Cryst. Growth 290 (2006) 207–212.
[55] E. Baudrin, S. Denis, F. Orsini, L. Seguin, M. Touboul, J. Tarascon, On the synthesis of monovalent, divalent and trivalent element vanadates, J. Mater. Chem. 9 (1999) 101–105.
[56] M.B. Bellakki, T. Baidya, C. Shivakumara, N.Y. Vasanthacharya, M.S. Hegde, G. Madras, Synthesis, characterization, redox and photocatalytic properties of $Ce_{1-x}Pd_xVO_4$ ($0 \leq x \leq 0.1$), Appl. Catal. B: Environ. 84 (2008) 474–481.
[57] C. Hsieh, W. Fan, W. Chen, J. Lin, Adsorption and visible-light-driven photocatalytic kinetics of organic dye on Co-doped titania nanotubes prepared by hydrothermal synthesis, Sep. Purif. Technol. 67 (2009) 312.
[58] N. Todorova, T. Giannakopoulou, G. Romanos, T. Vaimakis, J. Yu, C. Trapalis, Preparation of fluorine-doped TiO2 photocatalysts with controlled crystalline structure, Int. J. Photoenergy (2008) 534038.
[59] C. Zhang, C. Wang, J. Li, K. Yang, Structural and electronic properties of Fe-doped $BaTiO_3$ and $SrTiO_3$, Chin. Phys. 16 (2007) 1422–1428.
[60] K. Liu, J.Y. Zhang, X. Wu, B. Li, B. Li, Y. Lu, X. Fan, D. Shen, Fe-doped and (Zn, Fe) co-doped CdS films: could the Zn doping affect the concentration of Fe^{2+} and the optical properties, Phys. B 389 (2007) 248–251.
[61] P. Maruthamuthu, M. Ashokkumar, Doping effects of transition metals on the photosensitization of the WO_3 particles, Solar Energy Mater. 17 (1988) 433–438.
[62] S.U.M. Khan, M. Al-Shahry, W.B. Ingler Jr., Efficient photochemical water-spliting by a chemically modified n-TiO_2, Science 297 (2002) 2243–2245.
[63] K. Nagaveni, M.S. Hegde, N. Ravishankar, G.N. Subbanna, G. Madras, Synthesis and structure of nanocrystalline TiO_2 with lower band gap showing higher photocatalytic activity, Langmuir 20 (2004) 2900–2907.
[64] K. Nagaveni, G. Sivalingam, M.S. Hegde, G. Madras, Solar photocatalytic degradation of dyes, Appl. Catal. B: Environ. 48 (2004) 83–93.
[65] G. Sivalingam, K. Nagaveni, M.S. Hegde, G. Madras, Photocatalytic degradation of various dyes by combustion synthesized nano anatase TiO_2, Appl. Catal. B: Environ. 45 (2003) 23–28.
[66] M.S. Hegde, G. Madras, K.C. Patil, Acc. Chem. Res. 42 (2009) 704–712.
[67] M.A. Rauf, S.S. Ashraf, Radiation induced degradation of dyes, J. Hazard. Mater. 166 (2009) 6–16.
[68] A.L. Linsebigler, G. Lu, J.T. Yates, Photocatalysis on TiO_2 surfaces: principles, mechanisms and selected results, Chem. Rev. 95 (1995) 735–758.